

# Simulation of Solar Wind Based on K-epsilon (k-ε) Turbulence Models

Yong Ming<sup>1, 2\*</sup>, Xiaomin Gan<sup>2</sup> and Huajun Wang<sup>1</sup>

<sup>1</sup>Geophysics Institute, Chengdu University of Technology, Chengdu Sichuan 610009, China;

<sup>2</sup>Chengdu Radio & TV University, Chengdu, Chengdu Sichuan 610051, China.

**Abstract.** The whole interplanetary space is full of solar wind, which is a charged high-velocity flux of particles ejected during coronal expansion. In consideration that solar wind is fluid, and it will be obstructed to generate turbulence when it is dispersed, k-ε turbulence models are selected by ANSYS FLUNT in this paper to simulate solar wind as it flows through a satellite, and the simulation results are analyzed, in order to better explore the impacts of solar wind upon the earth's satellites and promptly avoid the damages of solar wind to the satellites. The simulation results have certain practical significance for guiding surveys about impacts of solar wind upon the earth's satellites.

**Keywords:** Solar Wind; Turbulence Models; Simulation.

## 1. Research Background

The whole interplanetary space is filled with solar wind, which is a charged high-velocity flux of particles ejected during coronal expansion. These particles carry “frozen” magnetic fields and thus generate interplanetary magnetic fields. The high-velocity flux of particles arising from variable solar wind greatly impacts spatial environment of the earth. The solar wind will interact with the earth's magnetic field when it reaches the earth to cause geomagnetic and ionospheric storms. As a result, catastrophic events will take place. The earth's satellites of the solar-terrestrial space are also disturbed and destroyed by solar wind. Under serious circumstances, the earth's satellites may be out of control and crash. Hence, it is of great significance for exploring the simulation scenes of solar wind blowing through the earth's satellites.

In simulating solar wind, the wind is considered as fluid and generates turbulence during its dispersion. In consideration of turbulent kinetic energy (K) and turbulent dissipation rate of solar wind plasma, the scene of solar wind flowing through the earth's satellite is simulated in this study.

## 2. Turbulence Model

Models are divided into standard models, RNG models and realizable models. With transport equations of K (turbulent kinetic energy) and turbulent dissipation rate, all of these models are impacted by turbulent kinetic energy and turbulent dissipation rate incurred by average velocity, buoyant force, expansion and electromagnetic force and so on. These three types of models differ in: (1) ways for calculating turbulent viscosity, (2) turbulent Prandtl number and (3) ways for calculating transport equations as well as relationships between generated items and  $G_k$ .

Developed by introducing turbulent dissipation rate based on single-equation models, this model is widely used. In this mode, the turbulent dissipation rate is defined as follows:

$$\varepsilon = \frac{\mu}{\rho} \left( \frac{\partial u'_i}{\partial x_k} \right) \left( \frac{\partial u'_i}{\partial x_k} \right) \quad (1)$$

Turbulent viscosity ( $\mu_t$ ) may be expressed as a sum function:

$$\mu_t = \rho C_\mu \frac{k^2}{\varepsilon} \quad (2)$$

Where,  $C_\mu$  is an empirical constant, and expected to be 0.09 as recommended by Launder et al. In a standard k-ε model, k and ε are unknown. The turbulent kinetic energy is determined as follows:

$$\frac{\partial(\rho k)}{\partial t} + \frac{\partial(\rho k u_i)}{\partial x_i} = \frac{\partial}{\partial x_j} \left[ \left( \mu + \frac{\mu_t}{\sigma_k} \right) \frac{\partial k}{\partial x_j} \right] + G_k + G_b - \rho \varepsilon - Y_M + S_k \quad (3)$$

The turbulent dissipation rate (ε) is as follows:

$$\frac{\partial(\rho\varepsilon)}{\partial t} + \frac{\partial(\rho\varepsilon u_i)}{\partial x_i} = \frac{\partial}{\partial x_j} \left[ \left( \mu + \frac{\mu_t}{\sigma_\varepsilon} \right) \frac{\partial \varepsilon}{\partial x_j} \right] + C_{1\varepsilon} \frac{\varepsilon}{k} (G_k + C_{3\varepsilon} G_b) - C_{2\varepsilon} \rho \frac{\varepsilon^2}{k} + S_\varepsilon \quad (4)$$

$G_k$  is a term for turbulent kinetic energy incurred by mean velocity gradient,  $G_b$  is a term for turbulent kinetic energy induced by buoyant force,  $Y_M$  represents contribution of pulse expansion to compressible turbulence,  $C_{1\varepsilon}$ ,  $C_{2\varepsilon}$  and  $C_{3\varepsilon}$  are empirical constants,  $\sigma_k$  and  $\sigma_\varepsilon$  denote Prandtl numbers corresponding to turbulent kinetic energy ( $k$ ) and dissipation rate ( $\varepsilon$ ) respectively,  $S_k$  and  $S_\varepsilon$  are source terms defined by users.

RNG model intends to reflect the impacts of small scales by large-scale motions and corrected viscosity, in order to systematically delete these small-scale motions from governing equations. The  $k$  equation and the  $\varepsilon$  equation are quite similar to standard  $k$ - $\varepsilon$  model :

$$\frac{\partial(\rho k)}{\partial t} + \frac{\partial(\rho k u_i)}{\partial x_i} = \frac{\partial}{\partial x_j} \left[ \alpha_k \mu_{eff} \frac{\partial k}{\partial x_j} \right] + G_k + \rho \varepsilon \quad (5)$$

$$\frac{\partial(\rho \varepsilon)}{\partial t} + \frac{\partial(\rho \varepsilon u_i)}{\partial x_i} = \frac{\partial}{\partial x_j} \left[ \alpha_\varepsilon \mu_{eff} \frac{\partial \varepsilon}{\partial x_j} \right] + C_{1\varepsilon}^* \frac{\varepsilon}{k} G_k - C_{2\varepsilon} \rho \frac{\varepsilon^2}{k} \quad (6)$$

$$\left\{ \begin{array}{l} \mu_{eff} = \mu + \mu_t \\ \mu_t = \rho C_\mu \frac{k^2}{\varepsilon} \\ C_\mu = 0.0845, \quad \alpha_k = \alpha_\varepsilon = 1.39 \\ C_{1\varepsilon}^* = C_{1\varepsilon} - \frac{\eta(1-\frac{\eta}{\eta_0})}{1+\beta\eta^3} \\ C_{1\varepsilon} = 1.42, \quad C_{2\varepsilon} = 1.68 \\ \eta = (2E_{ij} \cdot E_{ij})^{1/2} \frac{k}{\varepsilon} \\ E_{ij} = \frac{1}{2} \left( \frac{\partial u_i}{\partial x_j} + \frac{\partial u_j}{\partial x_i} \right) \\ \eta_0 = 4.377, \quad \beta = 0.012 \end{array} \right.$$

Where,

By comparing RNG  $k$ - $\varepsilon$  equation with the standard  $k$ - $\varepsilon$  equation, the former is discovered to have several changes as follows: (1) By correcting turbulent viscosity, rotation of mean flow and rotational flow are taken into account. (2) A term is added to the  $\varepsilon$  equation to reflect the mainstream mean strain rate ( $E_{ij}$ ). Thus, the terms generated in the RNG  $k$ - $\varepsilon$  model are not only related to flow, but also functions of spatial coordinates for the same problem. After above improvements, RNG  $k$ - $\varepsilon$  model become more effective for responding to high strain rate and the extent to which a streamline is bent.

Realizable  $k$ - $\varepsilon$  model is an improved one of a standard model. In using a standard model, the extremely high mean strain rate would lead to a negative normal stress. In order that the flow can be in line with physical laws of turbulent flow, it is necessary to exert certain mathematical constraints upon such normal stress. To make sure that such constraint can be imposed, Realizable  $k$ - $\varepsilon$  models are exported as follows:

$$\frac{\partial(\rho k)}{\partial t} + \frac{\partial(\rho k u_i)}{\partial x_i} = \frac{\partial}{\partial x_j} \left[ \left( \mu + \frac{\mu_t}{\sigma_k} \right) \frac{\partial k}{\partial x_j} \right] + G_k - \rho \varepsilon \quad (7)$$

$$\frac{\partial(\rho \varepsilon)}{\partial t} + \frac{\partial(\rho \varepsilon u_i)}{\partial x_i} = \frac{\partial}{\partial x_j} \left[ \left( \mu + \frac{\mu_t}{\sigma_\varepsilon} \right) \frac{\partial \varepsilon}{\partial x_j} \right] + \rho C_1 E \varepsilon - \rho C_2 \frac{\varepsilon^2}{k + \sqrt{\nu \varepsilon}} \quad (8)$$

$$\left\{ \begin{array}{l} \sigma_k = 1.0, \sigma_\varepsilon = 1.2, C_2 = 1.9 \\ C_1 = \max(0.43, \frac{\eta}{\eta+5}) \\ \eta = (2E_{ij} \cdot E_{ij})^{1/2} \frac{k}{\varepsilon} \\ E_{ij} = \frac{1}{2} \left( \frac{\partial u_i}{\partial x_j} + \frac{\partial u_j}{\partial x_i} \right) \\ \mu_t = \rho C_\mu \frac{k^2}{\varepsilon} \\ C_\mu = \frac{1}{A_0 + A_S U^* k / \varepsilon} \\ A_0 = 4.0 \\ A_S = \sqrt{6} \cos \phi \\ \phi = \frac{1}{3} \cos^{-1}(\sqrt{6}W) \\ W = \frac{E_{ij} E_{jk} E_{kj}}{(E_{ij} E_{ij})^{3/2}} \\ E_{ij} = \frac{1}{2} \left( \frac{\partial u_i}{\partial x_j} + \frac{\partial u_j}{\partial x_i} \right) \\ U^* = \sqrt{E_{ij} E_{ij} + \overline{\Omega_{ij}} \overline{\Omega_{ij}}} \\ \overline{\Omega_{ij}} = \Omega_{ij} - 2\varepsilon_{ijk} \omega_k \\ \Omega_{ij} = \overline{\Omega_{ij}} - \varepsilon_{ijk} \end{array} \right.$$

Where,

In this paper, the flow of solar wind is simulated with standard models, because only turbulent kinetic energy and turbulent dissipation of solar wind are needed.

### 3. Realization of Simulation

Concerning simulation tool, the flow is simulated with ANSYS Fluent as follows:

Step 1: Set scaling rate of mesh and determine the unit of mesh scale to be centimeter. The settings are shown in Fig 1.

Step 2: For the selection of turbulent models, multiple choices are available from Fluent, including SA single-equation model, standard  $k-\varepsilon$  two-equation model, Realizable  $k-\varepsilon$  model, RNG  $k-\varepsilon$  model, Reynolds stress equation, large eddy simulation (LES), standard  $k-\varepsilon$  model and SST  $k-\varepsilon$  model. Since solar wind is ferrofluid that flows around the earth in a rather complicated way, standard two-equation models are chosen for simulating turbulent flows and standard wall functions are used in simulating the scenarios when solar wind flows through a satellite. The settings are shown in Fig 2 as follows.

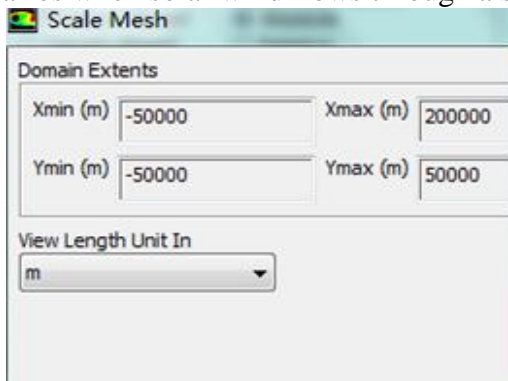


Fig 1. Settings of Mesh Scale

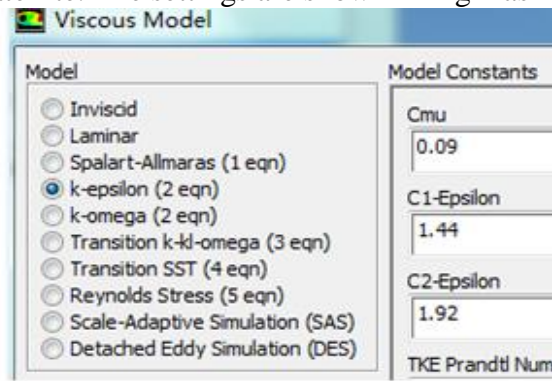


Fig 2. Setting of Turbulence Models

Step 3: Set discrete phase of DPM (Discrete Phase Model). In this paper, calculations are performed under vacuum environment, where particles are not impacted by any continuous phase or turbulent environment. Without evaporation and combustion, maximum calculation steps and integration step are directly set.

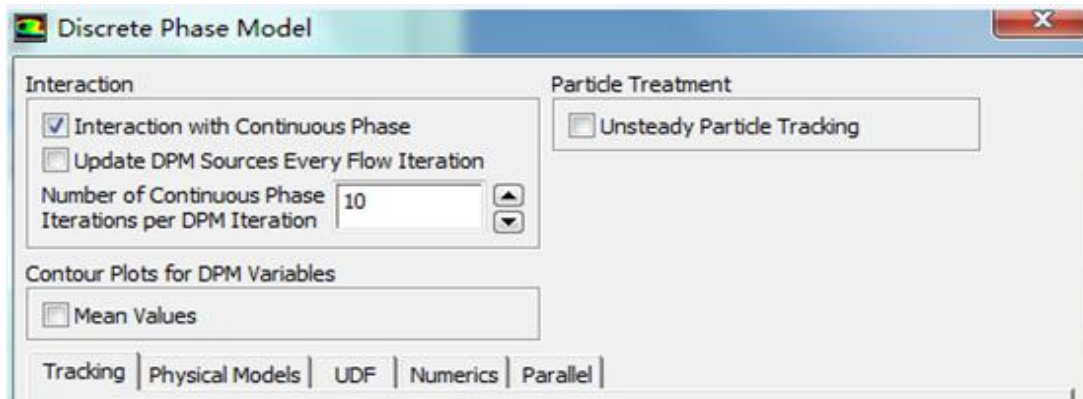


Fig 3. Setting of DPM

Step 4: Load a MHD model. Multiple computational models are available from Fluent. Some of these models can be directly operated on the GUI (graphical user interface), while the others can be operated through instructions. Enter `define/models>addon-module` into the text area by Fluent. Then Fluent hidden modules appear immediately, namely FLUENT Addon Modules:

- 1) MHD Model
- 2) Fiber Model
- 3) PEM Fuel Cell Model
- 4) SOFC Fuel Cell Model

Enter “1” and click return to load the DHM.

```
define/models/addon-module
Fluent Addon Modules:
  0. None
  1. MHD Model
  2. Fiber Model
  3. Fuel Cell and Electrolysis Model
  4. SOFC Model with Unresolved Electrolyte
  5. Population Balance Model
  6. Adjoint Solver
  7. Single-Potential Battery Model
  8. Dual-Potential MSMD Battery Model
Enter Module Number: [0] 1
Fast-loading "D:/ANSYS1~1.0/ANSYSI~1/v160/Fluent/Fluent16.0.0/addons/mhd\lib\
```

Fig 4. Loading of DHM (Data Handling Module)

Step 5: Set DHM. The magnetic field of the outer space is stable constant magnetic field, and prepared document on boundary conditions of a magnetic field is read.

Step 6: Read UDF. Particles move in the outer space and only bear electromagnetic force. The body force is set as electromagnetic force by modifying fluent source terms with UDF.

Step 7: Set boundary conditions. Particles depart from inlet boundary conditions and reach the earth through the outer space. Set departure speed and type of particles. The computational domain is vacuum environment, so it is unnecessary to couple with continuous phases.

Step 8: Set accuracy of algorithms and differentials. Set differential accuracy by SIMPLE algorithm. The solar wind runs in the outer space in a complicated way, so the first-order accuracy is selected in all cases, to make it convenient for calculating convergence.

Step 9: Initialization and solution. The computational domain is initialized and belongs to vacuum environment. Set computational steps and starts the calculation. Post-processing is performed after the calculation of convergence, to read all distributions within the computational domain.

#### 4. Conclusion

Fig 5 shows the simulation of the scenario when solar wind sweeps the earth’s satellites. The small cube represents a satellite located on a high orbit. At the intense outbreak of solar wind, the inner boundary of the earth’s outer radiation belt moves from 3R-4R (R is earth radius) to 2R, because the magnetosphere is compressed on the earth. The original space covered by the magnetosphere is shortened and narrowed. Besides, there is a significant increase in flow of electrons and protons inside

the satellite orbit. The high-orbit satellites face the risks of direct exposure to interplanetary space. As a result, the probability radiation damages increases drastically.

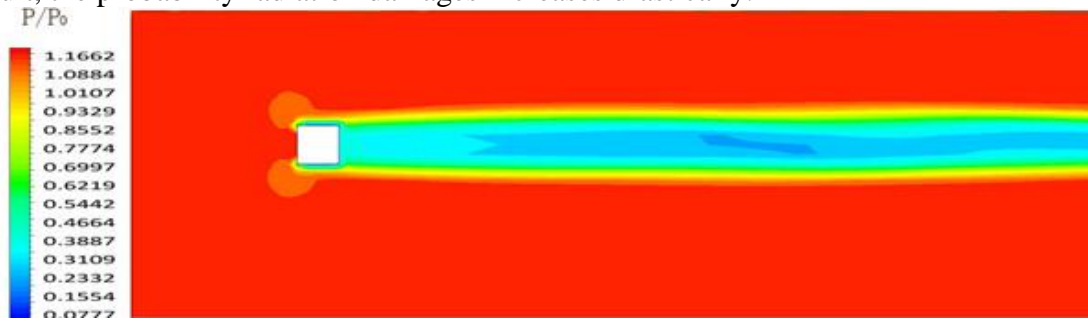


Fig 5. The Simulation of the Scenario When Solar Wind Sweeps the Earth's Satellite

It may be discovered from Fig 5 that areas of the satellite exposed to the sun are swept extremely intensely by solar wind, where the electron and proton fluxes moving in high speed may result in state blip of controllers (e.g. digital circuits, DSP, FPGA and ARM), abnormal operations caused by device interruption, and even permanent physical damages to satellite devices. The outbreak of high-speed solar wind may lead to compression of magnetosphere and exposure the satellite to the interplanetary space. The spacecraft running in the outer space uses the earth's magnetic field for posture positioning, assisted positioning or the rotational momentum is unloaded by geomagnetic torque. When solar wind intensively moves, drastic changes happen to the geomagnetic field. As a consequence, errors occur to pointing direction and posture control of the satellite. At last, the satellite may go out of control and even crash.

## References

- [1]. Jiang C Feng X, Wu S T et al. *Astrophysical Journal*, 2012, 759(2): 85
- [2]. Gonzalez W, Joselyn J, Kamide Yf et al. *Journal of Geophysical Research*, 1994, 99(A4): 5771
- [3]. Zhang J, Dere K P, Howard R A, et al. *Astrophysical Journal*, 2003, 582(1): 520
- [4]. Gui B, Shen C, Wang Y, et al. *Solar Physics*, 2011, 271: 111
- [5]. Shen Ct Wang Y, Gui B, et al. *Solar Physics*, 2011, 269(2): 389
- [6]. Wei F, Dryer M. *Solar Physics (ISSN 0038-0938)*, 1991, 132: 373